Flame Spread Experiments on a Horizontal Preheated Cable Layer

Pascal Zavaleta, Romain Meinier, Sylvain Suard, Rodolphe Sonnier, Laurent Ferry

Flame Spread Experiments on a Horizontal Preheated Cable Layer

*Pascal Zavaleta**, *Romain Meinier and Sylvain Suard, Fire Test Laboratory, Institute for Radiation Protection and Nuclear Safety (IRSN), 13115 St Paul-Lez-Durance, France*

Rodolphe Sonnier and Laurent Ferry, Polymers Composites and Hybrids (PCH), IMT Mines Ales, Ales, France

Abstract. Electrical cables are one of the main fire hazards in nuclear power plants (NPPs) and in many other industrial sectors. To assess the potential damages of the cable fires, models are required to forecast the fire spread over multiple cable trays and the resulting heat release rate. A new test device, called CISCCO, was developed to conduct flame spread experiments on a preheated horizontal cable layer to support the development and validation of the models. The characteristics of the CISCCO device are first presented before the description of four series of experiments that first investigated the temperature dependence of the flame spread velocity. The series involved a cable layer composed of either a polyvinyl chloride (PVC)-based cable, named PVC cable or a halogen free flame retardant (HFFR) poly(ethylene–vinyl acetate)/polyethylene-based cable, labelled HFFR cable. Temperature measurements performed in the solid phase (cable outer sheath) and in the gas phase (above the cable layer) allowed to assess the preheated cable layer temperature and the flame spread velocity. A first attempt of flame heat flux measurements was also conducted in this work. All series highlighted a temperature dependence of the flame spread velocity according to experimental power laws. The flame spread velocities were measured higher for the PVC cable (0 to 5.5 mm/s) than for the HFFR cable (0 to 1.5 mm/s) while the related preheated cable temperatures suitable for spreading were measured lower for the former (170 to 250°C) than for the latter (280 to 370°C). Finally, one of the four test series that used the PVC cable and implemented heat release rate measurements, revealed that the cable fire growth rate is also temperature dependent according to a power law and is linearly correlated to the flame spread velocity.

Keywords: Electrical cables, Fire experiments, Flame spread, Heat release rate, Temperature dependence

* Correspondence should be addressed to: Pascal Zavaleta, E-mail: pascal.zavaleta@irsn.fr

1. Introduction

Electrical cables are one of the main fire hazards in many industrial sectors such as buildings, aircraft, spacecraft, and nuclear power plants (NPPs) [1]. Several hundred kilometers of electrical cables can be found in most industrial plants that contain numerous electrical devices (electrical cabinets, digital switch racks, …) and multiple cable trays connecting these appliances. The electrical equipment and cables pose a potential source of fire since they contain both combustible materials and live electrical circuits. Almost half of the fire events in NPPs reported in the OECD FIRE Database were initiated in electrical equipment [2]. This kind of equipment can undergo electrical failures, such as a short circuit, overheating, or electrical arcing [3], which first ignite plastic materials of both electric wires and cables. To assess the potential damages of the cable fires on safety-related equipment, fire safety analyses need tools that can forecast the fire spread over multiple cable trays and the resulting heat release rate. To this end, previous works [4, 5] revealed that the knowledge of the flame spread velocity on grouped electrical cables, as found in cable trays, is of prime importance. In the continuity of these studies, the present work aims at especially studying the flame spread on horizontal cable trays since this configuration is the most common cable tray set-up found in NPPs [6].

Flame spread on solid is traditionally classified as wind-aided (concurrent) flame spread or opposed flow (counter-current) flame spread [7–9]. The former concerns flame spread in the same direction as ambient flow and is faster and more hazardous than the latter. The concurrent or opposed flow can be an external wind (meteorological in nature, from a mechanical ventilation…) or induced by the spreading flame itself due to buoyancy effects (natural convection). Thus, the latter effects could create an opposed flow for downward or lateral spread on a wall or for horizontal spread on a surface [10] while a concurrent flow can be generated as flame spreads upward along a wall or under a ceiling [8]. Furthermore, a significant number of works investigated the flame spread on single electric wire such as, e.g., the studies [11–13]. These works show that the flame spread along a horizontal cable wire is strongly impacted by the heat transfer ahead of the flame through the core. These studies also highlighted the impact of the insulation dripping on the flame spread, especially for a vertical orientation of the cable wire. Otherwise, few investigations studied in detail the flame spread along grouped electrical cables as found in cable trays of industrial facilities. A first work [14] addressed the flame spread on electrical cables that were placed on a vertical cable tray. This study used a flame spread apparatus for the measurement of vertical flame spread rates at different ambient temperatures. To this end, a 2-m long vertical sample is pre-heated with air to the desired temperature and ignited from its lower end with a small propane burner. The experiments showed that the vertical flame spread velocity is temperature dependent according to power laws and significantly changes with the studied electrical cable types. In contrast, the efforts [13] that were recently conducted to study the horizontal flame spread on flame retardant cables, showed that the spread was unsteady. The authors supposed that the complex cable composition (several sheaths made of

different materials) or the multiple thermal degradation phenomena (softening, melting, swelling…) could explain the unstable flame front and making these studies challenging, especially those dedicated to the investigations of horizontal flame spread.

Accordingly, given the lack of data and knowledge regarding the horizontal flame spread on electrical cables, the CISCCO (Cable Ignition and Spreading under Controlled COnditions) test device was developed for collecting data that will be used to support the development and validation of flame spread models. Many works [8, 10, 13–15] highlighted the impact of the fuel preheating (due e.g., to far-field convective and radiative effects of the fires) on the flame spread. So, the new apparatus was specifically designed to study the impact of the cable preheating on parameters such as the velocity of the flame spread on a horizontal cable tray and the heat release rate (HRR). This work presents the first flame spread experiments using the CISCCO test device. These experiments were organized in four test series. The two first ones were conducted as part of the study [16] that was followed by a complementary work that involved the two last series.

This works first describes the CISCCO test device and the related instrumentation. The second part presents the specifications of the experiments and in particular the test matrix, the electrical cables used, the test protocol and how the main studied parameters are assessed from the measurements. Next, flame spread theory leading to simplified formulations of the flame velocity for opposed flow flame spread and thermally thick materials, is briefly mentioned in the third part. Finally, the main part of this work presents and discusses the outcomes of the flame spread experiments. First, the temperature dependence of the flame spread velocity and the cable fire HRR, according to power laws are especially discussed, before highlighting a linear correlation between the flame spread velocity and the cable fire growth rate.

2. The CISCCO Flame Spread Test Device

2.1. Test Device

The overall set-up of the CISCCO device, shown in Figure 1, is composed of two functional zones: the exposure and fallback zones, both 1.7 m long. The exposure zone is the region where the horizontal cable layer is exposed to heat fluxes emitted by the radiant panels. For this work, the two pairs of radiant panels were placed in the exposure zone during all tests. The fallback zone can host the two radiant panels after and before a test to get easy access to the cable layer and the related sensors. For this purpose, two chain-driven motorized systems allow to move independently the two pairs of radiant panels. Figure 2 gives a top view of the cable layer with, e.g., the working lower radiant panels while the upper ones were removed in the fallback zone. The radiant panels aim at simulating the thermal effects of surrounding burning cable trays on the studied cable layer by controlling the heat fluxes imposed overall the cable layer, as further detailed (Sect. 3.2). These panels were especially designed to ignite the cables on a 20 cm long part of the studied cable layer, called the ignition area, and to preheat in a

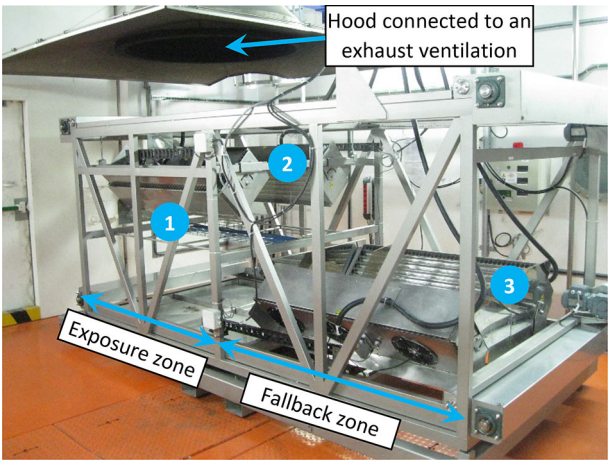

Figure 1. Overall set-up of the CISCCO flame spread test device with the cable layer (1), the upper (2) and lower (3) pairs of radiant panels shown in this picture in the exposure and fallback zones, respectively. The two pairs of radiant panels were placed in the exposure zone during all tests.

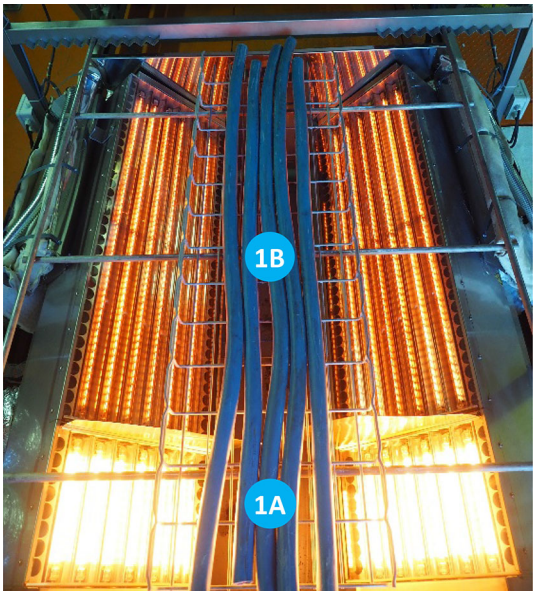

Figure 2. Top view showing the cable layer and the lower pair of working radiant panels in the exposure zone while the upper pair one was removed in the fallback zone. Ignition (1A) and spread (1B) areas.

controlled way the cables on the 80 cm long another part, named the spread area (Figure 2). Each panel is therefore composed of two parts, each equipped with six halogen lamps that emit in a spectrum range that spreads from 0.5 μm (visible) to 4.5 μm (start of the mid-infrared region) [17]. The smaller part of the radiant panels provides on the ignition area an incident heat flux (IHF) up to 70 kW/m^2 for igniting the cables while the longer one supplies on the spread area an IHF up to 30 kW/m^2. The latter heat fluxes allow to preheat the cable outer sheath, prior to the passage of the flame front, for studying the cable preheating impact on fire spread along the cable layer. The maximal preheated sheath temperature, obviously lower than their ignition temperature, depends on the cable type and will be specified further (see Sect. 5.1). Finally, given the different IHFs that can be imposed in the ignition and spread areas, a 20 cm long transition area can exist between the two previous zones where significant IHF gradients can be applied, as further shown.

Before each test series, heat flux cartographies were conducted to control the homogeneity of IHF over the ignition and spread areas. For this purpose, a cartography panel (Figure 3), that can host Gardon water-cooled total heat flux sensors, was successively exposed to the lower and upper pairs of radiant panels that usually work at 44 and 88% of their maximal electrical power. Figure 4 provides, e.g., the heat flux cartography that was performed over the upper surface before series3 for the higher setpoint of 88%. To obtain this cartography, IHF measurements were first performed with the dedicated plate in the position seen in Figure 3 and then turned it to allow additional measurements for new locations. Finally, for completing the cartography in the ignition area of five additional measurements, the plate was first moved of 10 cm to match its first hole line with the location X = 0 (three new measurements), before being finally turned (two new measurements).

The homogeneity of IHF is controlled for the ignition and spread areas with the homogeneity parameter, H [16], expressed in%:

$$H = \frac{2 \times \sigma}{\mu} \times 100 \tag{1}$$

where μ and σ are respectively the average value and the standard deviation of IHF measurements over the ignition and the spread areas, both expressed in kW/m^2. 2σ in Equation (1) specifies the expanded uncertainty of IHF distribution, meaning that the measured IHFs fall in the $[\mu - 2 \times \sigma, \mu + 2 \times \sigma]$ range over all the considered area with a confidence level of 95%. For the example of cartography seen in Figure 4, H was assessed at 6% over the 20 cm long ignition area and a width of 30 cm, with an average IHF of 64 kW/m^2 [16]. IHFs thus fall in the 60 to 68 kW/m^2 range over all the ignition area with a confidence level of 95%. For the same example of cartography (Figure 4), H was evaluated at 11% over the 80 cm long spread area and a width of 30 cm, with an average IHF of 25 kW/m^2. IHFs thus fall in the 22 to 28 kW/m^2 range over all the spread area with a confidence level of 95%. These outcomes show a satisfactory homogeneity of IHF over a width larger than the wider cable layer used in this work (22 cm). The cartogra-

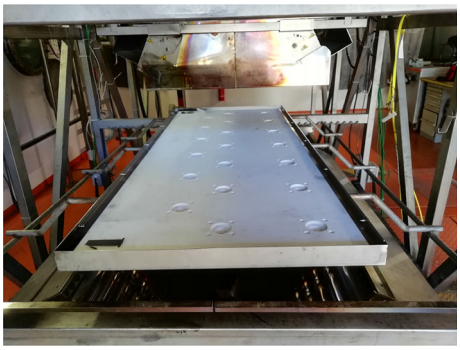

Figure 3. Cartography plate used to support the heat flux cartographies.

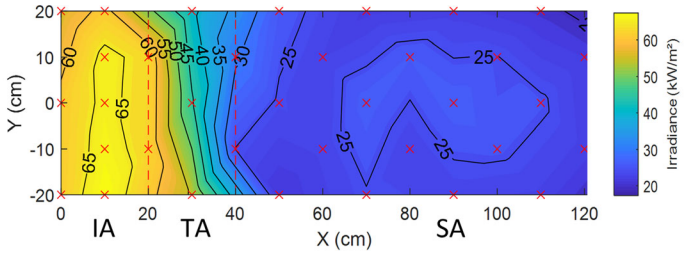

Figure 4. Heat flux cartography over the 120 cm long and 40 cm wide upper exposed surface. *IA* ignition area, *TA* transition area, *SA* spread area. The red crosses give the locations of IHF measurements. The dashed lines specify the borders between the ignition, transition and spread areas.

phies also led to determine the length (20 cm) of the transition area that exists between the ignition and spread areas (Figure 4).

2.2. *Instrumentation*

Figure 5 shows an example of a cable layer equipped with 12 pairs of 1.5 and 1 mm K-type thermocouples, separated from each other by 10 cm, between $X_1 = 10$ cm and $X_{12} = 120$ cm. The twelve 1.5 mm K-type thermocouples ($T_s\_X_i$, $i = 1$ to 12) were inserted by 1 to 2 mm in the cable sheath for measuring the solid phase temperature while the 1 mm K-type thermocouples ($T_g\_X_i$, $i = 1$ to 12) were placed nearly and above the cable layer for measuring the gas phase temperature. Figure 6 shows the Gardon heat flux sensor placed at the cable layer extremity, opposite to the ignition area.

This gauge aims at measuring the total incident heat flux (TIHF) that includes the flame ($\left(\dot{q}''_f\right)$ and radiant panel (IHF) heat fluxes incident to the cable layer. In this study, this sensor was only used during two experiments to preserve it given

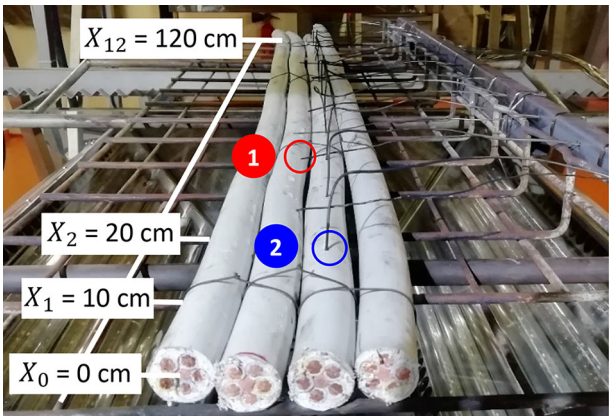

Figure 5. Temperature measurements performed in the gas phase (above the cable layer (1)) and in the solid phase (cable outer sheath (2)).

Figure 6. The Gardon water-cooled heat flux sensor (3) placed at the cable layer extremity.

its contact with flames when they reach its location. Cameras were used to follow the spreading of the flame front along the cable layer from the side and top views. Furthermore, for the last test series, concentrations of carbon dioxide, carbon monoxide and oxygen, gas temperature, volume flow rate and relative pressure

were also measured in the exhaust ventilation duct connected to the hood located above the CISCCO test device (Figure 1). These measurements allowed assessing the HRR for all tests of the last series. Figure 7 provides the schematic diagram of the CISCCO test device including all instrumentation above described.

3. Presentation of the Experiments

3.1. Test Matrix and Objectives

Table 1 provides the test matrix of the first flame spread experiments on a horizontal cable layer, that used the CISCCO device. This device was placed in a large-scale facility where the conditions are similar to open atmosphere conditions.

All test series used one layer of tight cables, as depicted in Figure 5. The first three series used a 11 cm wide cable layer while the last one involved a 22 cm wide cable layer. Series1, 3 and 4 used the same polyvinyl chloride (PVC)-based cable, named PVC cable, while series2 used a halogen free flame retardant (HFFR) poly(ethylene–vinyl acetate)/polyethylene (EVA/PE)-based cable, labelled HFFR cable. The main characteristics of these cables are specified in Table 2. The properties of the outer sheath of the two cables were determined in previous works [18, 19] that also showed that these sheaths were thermally thick materials. The PVC cable is considered as a low qualified (LQ) cable since it only meets the requirement of the IEC/EN 60332-1-2 standard test [20] that is not challenging regarding the cable reaction to fire. Note that this standard test corresponds to the Eca class of the recent Euroclass EN 50575 [21], as specified in Table 2. Conversely, the HFFR cable is stated as a well-qualified (WQ) cable since it satisfies more demanding cable reaction to fire standards regarding the fire spread (IEC/EN 60332-3-23 [22] and NF C 32-070 (C1) [23]) and also standard tests related to smoke density and acidity (IEC/EN 61034-2 [24] and 60754-2 [25], respectively). For the WQ cable, its class according to the Euroclass EN 50575 is unknown.

As previously mentioned, the overall objectives of this work were to investigate the impact of the cable preheating on the flame spread on a horizontal preheated cable layer. The studied flame spread parameters were especially the flame spread velocity and the heat release rate. Furthermore, additional goals were also pursued such as the study of the impact on the flame spread of the cable type (the LQ PVC cable for series1&3 vs the WQ HFFR cable for series2) and the cable layer width (11 cm for series1&3 vs 22 cm for series4). A last specific purpose was to check the consistency of series1 and series3 that were specified identically but the former was conducted in 2020 [16] and the latter in 2022.

3.2. Test Protocol

The test protocol of the CISCCO experiments successively includes the preheating, ignition, spread and decay stages, as illustrated in Figure 8 by TIHF and the sheath temperature measured at the cable layer extremity (Figure 6). The first stage aims at pre-heating the cables up to the desired setpoint temperature measured at the centre of the spread area (i.e., $X = 80$ cm) by an optical pyrometer.

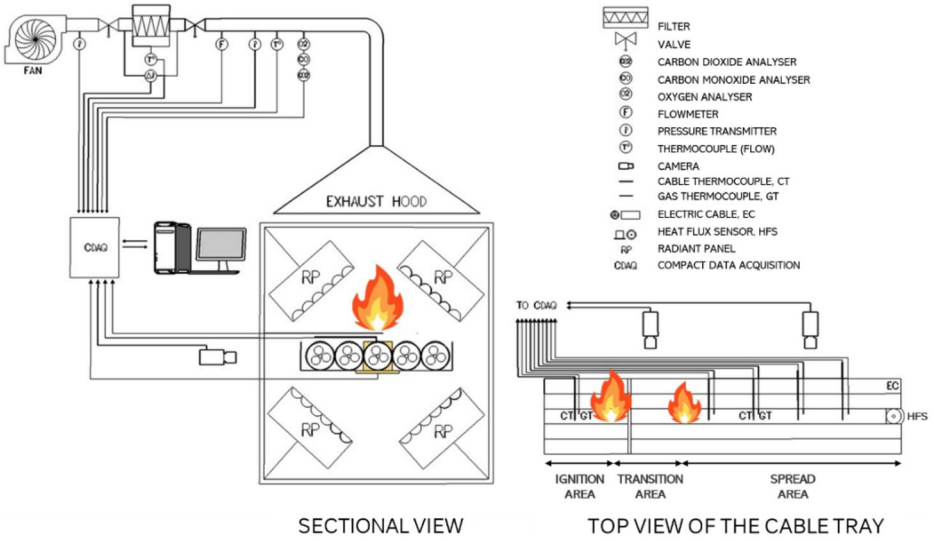

Figure 7. Schematic diagram of the CISCCO test device.

Table 1
Test Matrix of the Flame Spread Experiments

Test series	Cable layer width [cm]	Cable type	Number of tests
Series1	11	PVC	11
Series2	11	HFFR	18
Series3	11	PVC	9
Series4	22	PVC	10

PVC polyvinyl chloride, *HFFR* halogen-free flame retardant

This pre-heating was performed according to a temperature ramp that was fixed at 6.5°C/min for this study and controlled by an automaton that relied on the cable layer surface temperature measurements provided by the optical pyrometer. Note that to reach the thermal equilibrium of the outer sheath, the preheating stage was extended of 5 min once the preheated temperature setpoint is achieved. The value of the temperature ramp (6.5°C/min) was estimated from gas temperatures measured close to electrical cables during real-scale fire tests [26] that led to assume a plausible outer sheath temperature of about 200°C after a 30-min fire duration. The preheating stage aims at reproducing the cable preheating before their ignition as it occurred in multiple cable tray fire tests [6] when the cables are preheated by far-field convective and radiative effects of the fire [8]. Next, the ignition phase starts by the very fast increase of IHF imposed on the ignition zone up to a value that can vary between 30 kW/m^2 and 70 kW/m^2 according to the cable type (Figure 9A). Few seconds to few 10 s later, an electrical igniter provokes the

Table 2
Specification of the Cables Used for the Flame Spread Experiments

Cable ID	 PVC cable	 HFFR cable
Cable reference	Low voltage cable NYM-J 5 G 25 mm^2 (RM)	Low voltage cable 74C068 SH P 3X2.5 Cu2 K1 NA
Cable diameter (mm)	28	12
Main non-metallic materials	PVC, PE, $CaCO_3$ and plasticizer	EVA, PE and ATH
Properties of the cable outer sheath		
Thickness (mm)	2	2.5
Thermal conductivity, k(W/(m.K))	0.23	0.50
Density, ρ (kg/m^3)	1520	1540
Specific heat, C_p(J/(kg.K))	1110	1520
IEC and NF cable reaction to fire standard tests	IEC 60332-1-2 (EN 50575-Eca)	NF C 32-070 (C1), IEC 60332-1-2, IEC 60332-3-23, IEC 61034-2, IEC 60754-2

ATH aluminium tri-hydroxide, *$CaCO_3$* calcium carbonate, *EVA* poly(ethylene–vinyl acetate), *HFFR* halogen free flame retardant, *PE* polyethylene, *PVC* polyvinyl chloride, *IEC* international electrotechnical commission, *NF* norme Française

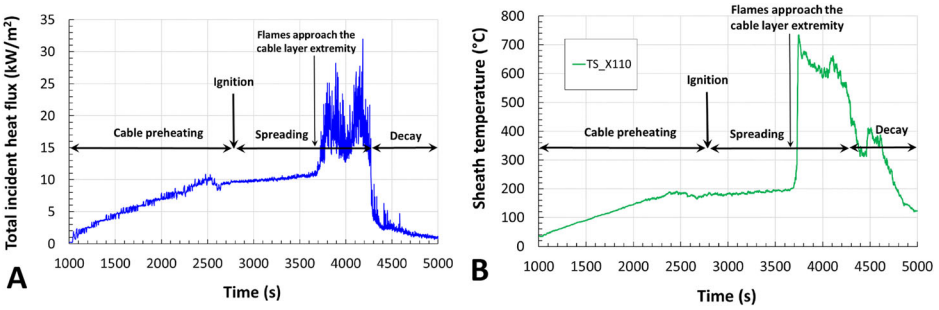

Figure 8. Test protocol illustrated by the total incident heat flux (A) and the sheath temperature (B) measured at the cable layer extremity (the cable layer length was reduced to 1.1 m for the two tests that used a heat flux sensor in order to allow its implementation).

cable ignition in this 20 cm long zone (Figure 9B). Then, when the flame front reaches the position located at 40 cm from the extremity of the ignition zone, which is the border between the transition zone and the spread zone (Figure 4), the spreading stage starts. Flame spreads up to the cable layer extremity located at 120 cm from the start of the ignition area, as depicted in Figure 10. During the ignition and spread stages, the radiant panels provide a constant heat flux on the spread area, as seen in Figure 8A before the arrival of the flame front. Finally, the

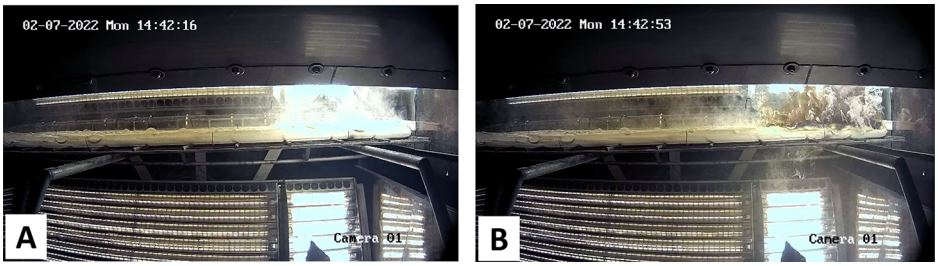

Figure 9. Ignition stage of the cable layer (seen from camera 1). (A) Increase of IHF imposed on the ignition zone. (B) Ignited cable layer in the ignition zone.

Figure 10. Spreading stage. Flame front at X = 40 cm (A seen from camera 1) and at X = 120 cm (B seen from camera 2).

fourth and last stage (decay stage) starts after the shutdown of the four radiant panels.

The use of these radiant panels offers several advantages for CISCCO experiments, such as the rapid achievement of IHF setpoints, the homogeneous radiation over distinct areas and the easy control of the cable heating. However, given the emission of the halogen lamps from the visible (0.5 μm) up to the start of the mid-infrared region (4.5 μm), as previously mentioned, the absorbance (part of the heat flux emitted by the source which is absorbed by the material), can be different for samples exposed in the CISCCO device than those used, e.g., in the cone calorimeter for which the electric heater fully emits in the mid-infrared region [27]. This discrepancy was clearly observed in the latter work for clear PMMA which weakly absorbs radiation in the near infrared, but less pronounced for electrical cables [16]. For example, the latter study assessed for the studied HFFR cable an absorbance of about 0.72 and 0.84 when it was exposed to the CISCCO device lamps and the cone calorimeter heater, respectively. This can imply some differences, e.g., on the time to cable ignition between the two above devices but with no significant impact on the current work for which the main goal was to conduct flame spread experiments on a preheated cable layer. To this end, besides the ignition of the cable layer in the ignition zone, the key purpose of the used radiant panels was to preheat the spread zone and maintain this preheating during the

whole spread stage. Afterwards, the spread was ensured by the flame itself given the heat transfer from flame to the unburnt cables, as fully described further.

3.3. Studied Parameters

This section presents how the main studied parameters are evaluated, from the measurements, on the first seventies centimeters of the spread area ($X = 40$ to 110 cm). The last portion of this area ($X = 110$ to 120 cm) was indeed not considered given boundary effects. The preheated sheath local temperature, $T_{ps}\_X_i$, with $i = 4$ to 11, due only to the external heating (radiant panels), must be evaluated before it is impacted by the heat flux of the progressing flame front. To this end, $T_{ps}\_X_i$ is obtained from the sheath temperature measured at the same location, $T_s\_X_i$, when the flame front approaches the previous location X_{i-1}. This is considered when the sheath temperature $T_s\_X_{i-1}$, measured at X_{i-1} reaches the value of 300°C ($t_{300°C\ at\ X_{i-1}}$), as illustrated in Figure 11. This evaluation assumes that the thermal influence of the flame front is negligible beyond 100 mm. Finally, for every experiment, the preheated sheath average temperature, T_s, is assessed from the eight $T_{ps}\_X_i$, such as follows:

$$T_s = \frac{1}{8}\sum_{i=4}^{i=11} T_{ps}\_X_i = \frac{1}{8}\sum_{i=4}^{i=11} T_s\_X_i(t_{300°C\ at\ X_{i-1}}) \tag{2}$$

The flame front position, X_f, is identified at every location X_i, with $i = 4$ to 11, when the related measured gas phase temperature, $T_g\_X_i$, reaches the value of 500°C ($t_{500°C\ at\ X_i}$). This threshold is indeed considered as a suitable criterion showing the presence of flame [28]. The flame spread local velocity, $Vf_{X_{i+1}-X_i}$, is assessed (in mm/s) as the ratio of the distance separating two thermocouples located in the gas phase (i.e., 100 mm) to the time required for the flame front to move between these two locations

$$Vf_{X_{i+1}-X_i} = \frac{100}{t_{500°C\ at X_{i+1}} - t_{500°C\ at X_i}} \tag{3}$$

Next, for every test, the flame spread average velocity, Vf, is assessed from the seven evaluations of $Vf_{X_{i+1}-X_i}$, such as follows:

$$Vf = \frac{1}{7}\sum_{i=4}^{i=10} Vf_{X_{i+1}-X_i} \tag{4}$$

Vf is also assessed from the temperatures measured in the cable sheath in the same way as above indicated. The final Vf is taken as the average of the two evaluations. Examples of the local flame spread velocities assessed from the temperatures measured in the gas phase and in the cable sheath are given in Figure 12. Furthermore, the HRR is calculated from the carbon dioxide generation (CDG) and the oxygen consumption (OC) calorimetry methods. Given that the CISCCO

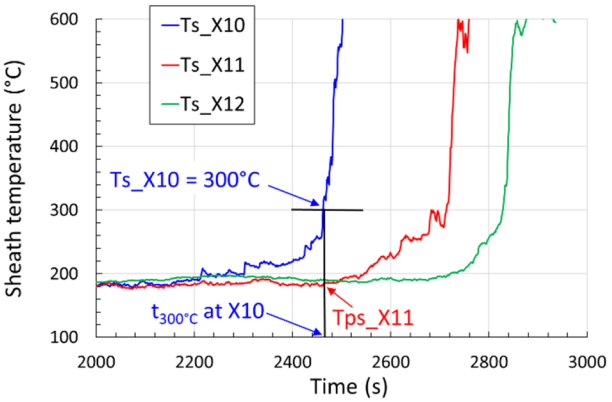

Figure 11. Measured sheath temperatures at three locations during the flame spread experiments and illustration of the method to assess, e.g., $T_{ps}\_X_{11}$, the preheated sheath local temperature at 110 cm from the cable layer extremity.

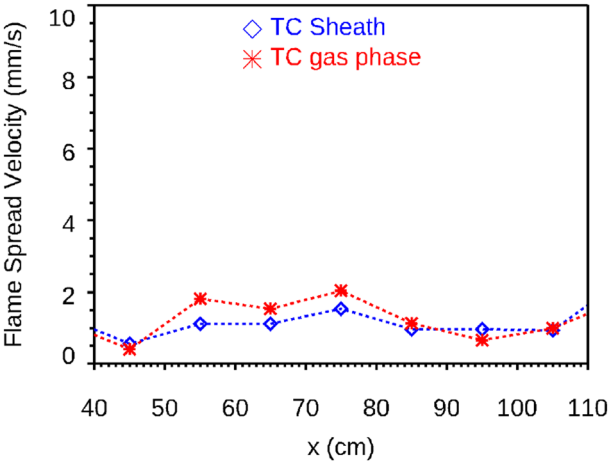

Figure 12. Example of flame spread local velocities assessed over the spread zone (X = 40 to 110 cm), from the temperatures measured in the gas phase and in the cable sheath.

experiments were conducted in open atmosphere conditions, the two evaluations $\dot{Q}_{CDG}$ and $\dot{Q}_{OC}$ were assessed considering negligible production of CO and soot species, as detailed in [29]. The final HRR ($\dot{Q}$) is then obtained as the average of the two previous contributions:

$$\dot{Q} = \frac{(\dot{Q}_{CDG} + \dot{Q}_{OC})}{2} \tag{5}$$

4. Flame Spread Theory

Visual observations of the flame front during its progress as part of the current experiments seem indicate that the flame front tends to lean towards the burning area. This suggests an opposed flow flame spread configuration, as ideally represented in Figure 13 [8]. The opposed flows would be induced by the spreading flame itself due to local buoyancy effects, as previously mentioned, and also by the smoke extraction[1] in the hood located above the CISCCO device (Figure 1). In addition, it was also noticed that the flame front sporadically leant towards the unburnt cable layer, but to a much lesser extent than the situations for which it tilted towards the burning area. An opposed flow flame spread regime is therefore assumed for the CISCCO experiments, even if the observed regime can occasionally differ from the ideal representation for opposed flow spread (Figure 13). The following now aims at briefly mentioning the simplified formulations of the flame velocity for an opposed flow flame spread. The flame spread is assumed steady and is depicted as being blown by a wind with a constant velocity V_g. The heat flux from the flame ($\dot{q}''_f$) that is applied over a distance, Δ, named the length of flame heating, is also supposed constant. Δ is the distance from the pyrolysis front at the ignition temperature, T_{ig}, to the region at the solid temperature, T_s, thermally not affected by the flame. However, T_s can be impacted by an external heating caused, e.g., by far-field convective and radiative effects of the fire, as already mentioned.

Considering the above assumptions and also thermally thick materials, Quintiere [8] proposed the following formulation for V_f:

$$V_f = \frac{4\left(\dot{q}''_f\right)^2 \Delta}{\pi(k\rho C_p)\left(T_{ig} - T_s\right)^2} \tag{6}$$

where k, ρ and C_p are the thermal conductivity, density and specific heat, respectively of the solid phase. Furthermore, deRis [10] proposed a formulation for V_f with consideration of the gas and solid phases:

$$V_f = \frac{V_g(k\rho C_p)_g\left(T_f - T_{ig}\right)^2}{k\rho C_p\left(T_{ig} - T_s\right)^2} \tag{7}$$

where T_f is the flame temperature (°C) and $(k\rho C_p)_g$ correspond to the product of the thermophysical properties (thermal conductivity, density and specific heat,

[1] Given the maximal extraction flow rate of 3000 m^3/h and the hood diameter of 1.5 m, the maximal average air velocity in the hood duct, before fire, was close to 0.5 m/s.

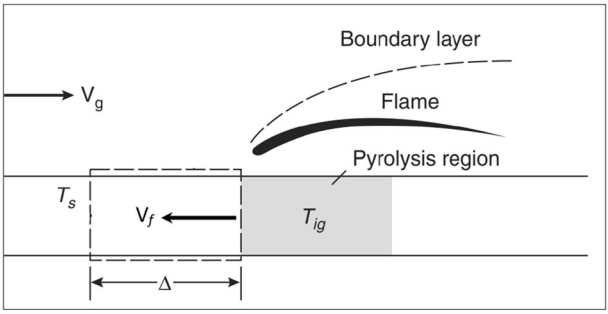

Figure 13. Illustration of the modelling of opposed flow flame spread on a horizontal solid [8]. Δ, distance from the pyrolysis front at the ignition temperature, T_{ig}, to the region at the solid temperature, T_s; V_f, flame spread velocity; V_g, wind velocity.

respectively) of the gas phase (g). In addition, DeRis and Quintiere [30] considered that for the specific configuration of lateral flame spread, the following equation, inspired by both Equations (6) and (7), can be useful for determining the essential parameters describing opposed flow flame spread parameters on thick materials:

$$V_f = \frac{\Phi}{k\rho C_p \left(T_{ig} - T_s\right)^2} \tag{8}$$

where Φ depends on V_g, the ambient oxygen concentration and the studied material. However, for limited velocities of natural convection flows (lower than 0.3 m/s [8]) in air, Φ is assumed constant for a given material.

5. Results and Discussion

This section presents the outcomes of the flame spread experiments and discusses the effect of the cable preheating on V_f and the HRR. Before it, Figure 14 shows pictures of the flame front development over the 22 cm wide cable layer (series4) when it reaches the locations X = 50, 70, 90 and 110 cm. This figure illustrates the slight deformation of the flame front that can occur during some experiments from around X = 90 cm (Figure 14C) and also observed beyond, at X = 110 cm (Figure 14D). However, the authors assume that this deformation of the flame front profile that remains moderate from X = 90 to 110 cm, does not change significantly the flame spread velocity (assessed from X = 40 to 110 cm, see Sect. 3.3) compared to that obtained when the profile is always flat. Such alteration could be due to a slight dissymmetry of the cable layer heating, despite the homogeneity of the incident heat flux evaluated at about 10% over the spread area (see Sect. 2.1).

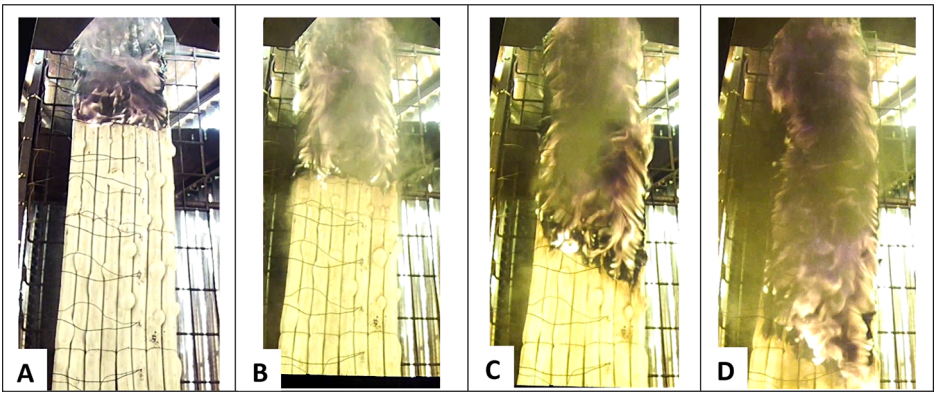

Figure 14. Illustration of the flame front development over the 22 cm wide cable layer (series4) at X = 50 cm (A), 70 cm (B), 90 cm (C) and 110 cm (D).

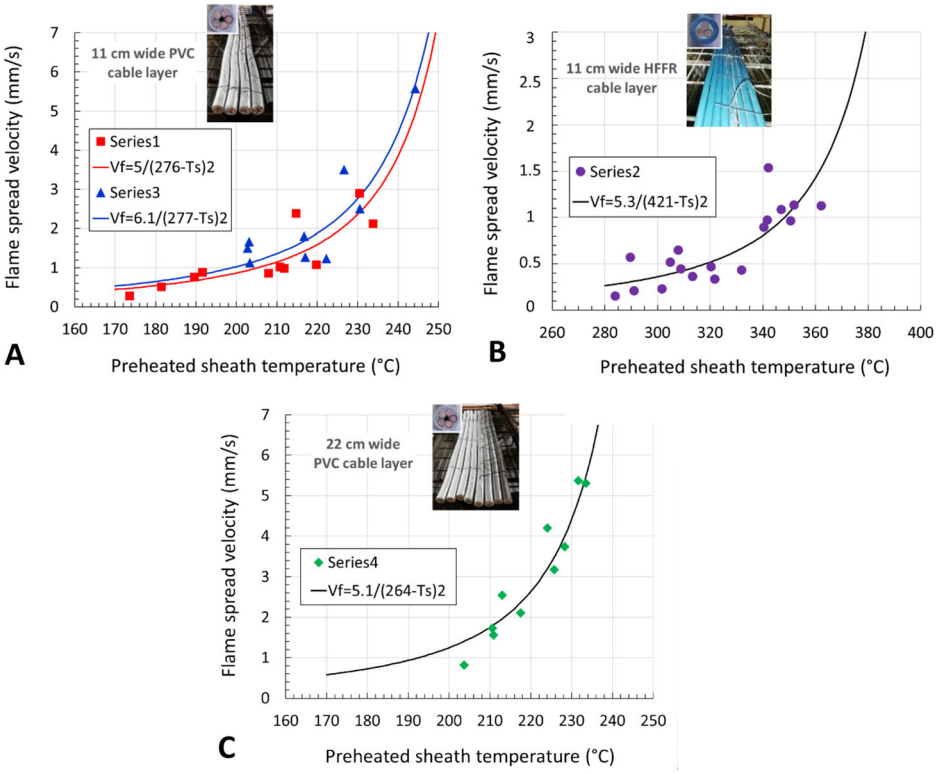

Figure 15. Flame spread velocity as a function of the preheated sheath temperature. (A) Series1&3. (B) Series2. (C) Series4.

5.1. *Effect of the Cable Preheating on the Flame Spread Velocity*

This section aims at studying the effect of T_s on V_f for the four test series (Table 1). The related data are shown in Figure 15 and for every series, a power law that fits the best the data, according to the least square method, is specified:

$$V_f = \frac{A}{(B - T_s)^2} \tag{9}$$

A and B values are given in Table 3 for the three studied cable layers. The similarity between the experimental laws (Equation (9)) and the theoretical one (Equation (8)) proposed for an opposed flow flame spread could therefore corroborate the assumption that this flame spread regime would best represent that obtained during the current experiments. Atreya et al. [15], that studied horizontal flame spread on wood samples, also found experimental laws for flame spread calculation similar to Equation (9), provided that the surface temperature (T_s) is defined as the temperature due to external radiation alone. This specification is the same than that defined in this study (Sect. 3.3) for the preheated sheath temperature (T_s).

Furthermore, the comparable experimental laws proposed for series1 and series3 (see Figure 15A and Table 3 for the A and B values), suggest a satisfactory consistency of these series that were specified identically, but performed at 2-year interval by distinct operators.

In addition, the B value for the HFFR cable layer of series2 (421°C, Table 3) is nearly the same than T_{ig} measured in the cone calorimeter (420°C) for the same cable [18]. Conversely, for the PVC cable, the comparison between the B value (around 270°C for the 11 and 22 cm wide PVC cable bundles, see Table 3) with T_{ig} measured in the cone calorimeter needs to be a little more commented. The latter measurement was indeed challenging due to the significant formation of char prior to the ignition of the PVC cable in the cone calorimeter [19]. Nevertheless, an "apparent" T_{ig} of about 320°C was determined in the latter work to be consistent with the experimental ignition delays that were impacted by the char formation. In the CISCCO experiments, the progressive increase of IHF applied on the cable layer during the preheating stage (contrarily to the immediate exposure to IHF setpoint in the cone calorimeter) did not lead to the formation of char prior to the ignition and spread stages. Otherwise, softening and swelling (Figure 14A) of the sheath were observed. Accordingly, the different thermal degradation states of the cables observed before their ignition in the CISCCO experiments and cone calorimeter could substantiate distinct T_{ig}. (around 270 and 320°C for the first and second test device, respectively).

To discuss further the consistency between the experimental (Equation (9)) and theoretical (Equations (6) and (8)) laws, the experimental values of A and V_f are compared with those obtained from below Equation (10) for A (deduced from Equations (6), (8) and (9)) and from Equation (6) for V_f.

Table 3
A and B Values of the Experimental Power Laws Giving the Flame Spread Velocity for the Three Studied Cable Layers

Parameter	11 cm wide PVC cable layer (series1&3)	11 cm wide HFFR cable layer (series2)	22 cm wide PVC cable layer (series4)
A (m/s.°C^2)	5 (series1) and 6.1 (series3)	5.3	5.1
B (°C)	276 (series1) and 277 (series3)	421	264

$$A = \frac{\Phi}{k\rho C_p} = \frac{4\left(\dot{q}''_f\right)^2 \Delta}{\pi\left(k\rho C_p\right)} \tag{10}$$

The theoretical values of A and V_f are calculated for the last test of series2 (11 cm wide HFFR cable layer) and the first one of series4 (22 cm wide PVC cable layer) that both implemented a heat flux sensor placed at the cable layer extremity (Figure 6). This sensor measured TIHF that includes $\dot{q}''_f$ and IHF, both incident to the cable layer, as earlier specified in Sect. 2.2. Figure 16 provides $\dot{q}''_f$ therefore deduced from the difference between TIHF and the constant IHF (since the end of the preheating stage) at 17.5 and 10.5 kW/m^2 for the related tests of series2 and 4, respectively.

In addition, $\dot{q}''_f$ is averaged over its growth period (t_{growth}) that ends at the first peak (Figure 16). This peak coincides with the arrival of the flame front at the cable layer extremity. The average $\dot{q}''_f$, $\overline{\dot{q}''_f}$, is thus evaluated at about 2 and 5 kW/m^2 for the last test of series2 and the first one of series4, respectively. The wider cable layer and the use of the low-qualified PVC cable for the latter test (instead of the well-qualified HFFR cable for the former test) could explain the above differences of $\overline{\dot{q}''_f}$ that will be used to assess V_f from Equation (6). Furthermore, in absence of flame heating length (Δ) measurements, this last one is fixed at 0.05 m, which corresponds to the half of the maximal flame front thermal influence length (0.1 m), that is assumed in this study (see Sect. 3.3). Finally, for the related tests of series2 and series4, T_s was measured at 362 and 204°C, respectively, and, as previously commented, T_{ig} is rounded to 420°C (HFFR cable) and 270°C (PVC cable), respectively. Accordingly, based on the above values of $\overline{\dot{q}''_f}$, Δ, T_s, T_{ig} and the thermophysical properties of the HFFR and PVC cables (Table 2), Equations (10) and (6) provide the theoretical values of A and V_f, respectively. For the first test of series4 (22 cm wide PVC cable layer), the calculated values of A (4.1 m/s.°C^2) and V_f (0.94 mm/s) are comparable to those obtained experimentally for A (5.1 m/s.°C^2, see Table 3) and V_f (0.82 mm/s measured for T_s = 204°C, see Figure 15C). This shows the consistency of the experimental law (Equation (9)) and the theoretical ones (Equations (6) and (8)) for this test using a PVC cable. In contrast, for the last test of series2 (11 cm wide HFFR cable layer), the calculated

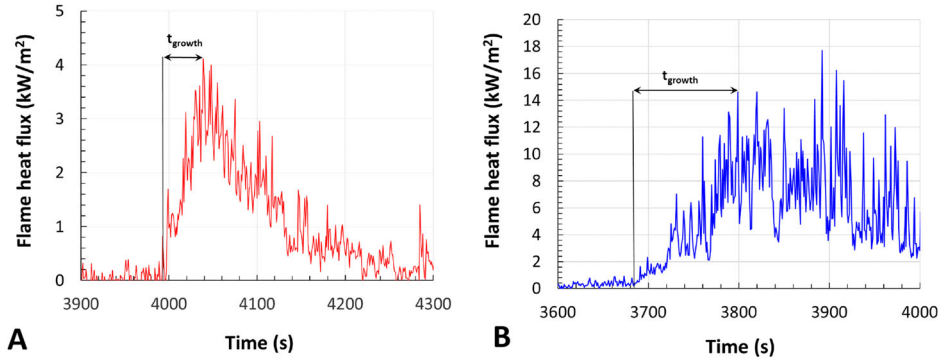

Figure 16. Flame heat flux incident to the unburnt cables and measured at the cable layer extremity. (A) Last test of series2 (11 cm wide HFFR cable layer). (B) First test of series4 (22 cm wide PVC cable layer).

values of A (0.2 m/s.℃^{2}) and V_f (0.06 mm/s) are significantly lower than those obtained experimentally for A (5.3 m/s.℃^{2}, see Table 3) and V_f (1.12 mm/s measured for T_s of 362℃, see Figure 15B). One explanation to substantiate such discrepancy is related to the change of the thermophysical properties of the cable outer sheaths when they are exposed to an external heat flux [31, 32]. This is especially true for the outer sheath of the HFFR cable for which the mass content of the ATH flame retardant (Table 2), initially of about 60% [18], should clearly decrease due to its dehydration [33] that occurs during the preheating of the sheath up to about 360℃. Accordingly, after this stage, the outer sheath density is supposed clearly lower given the density of ATH at 20℃ (2400 kg/m^3 [33]) higher than those of EVA and PE materials (both close of 1000 kg/m^3 [33]). In addition, Girardin et al. [31] showed that the thermal conductivity of a EVA/ATH mixture significantly decreased up to about 0.2 W/(m.K) at 400℃. Finally, it is also assumed that the cable preheating up to 380℃ could start to degrade the polymeric materials (EVA, PE) of the outer sheath, which could decrease T_{ig} compared to that measured in the cone calorimeter for the studied HFFR cable (420℃) [18]. Accordingly, it is suggested to consider in Equations (10) and (6), a lower value for T_{ig} arbitrarily set at 400℃, and the values of 0.2 W/(m.K) and 1000 kg/m^3 for k and ρ, respectively, that could be similar to those obtained after the preheating up to about 360℃. These equations therefore give the values of 0.84 m/s.℃^{2} for A and 0.6 mm/s for V_f while the experimental values for the HFFR cable are equal to 5.3 m/s.℃^{2} and 1.12 mm/s, respectively, as above mentioned. Thus, despite the change of the cable sheath property values, the discrepancy between the experimental and theoretical values remains significant for the HFFR cable type. Future work are therefore required for such cable type and could especially include efforts devoted to the measurements of $\overline{\dot{q}''_f}$ and Δ, that are also essential to a proper assessment of A (Equation (10)) and $V_f(Eq.((6))$. These works will also

allow to consolidate for another PVC cable types the satisfactory outcome obtained for the studied PVC cable.

Moreover, Table 4 reports additional outcomes of the temperature dependence of the flame spread velocity such as the minimal sheath temperature allowing flame spread [8], $T_{s,min}$, that was experimentally determined for the three studied cable layers (Figure 15). This parameter is notably lower for the 11 cm wide PVC cable layer (170°C) than for the 11 cm wide HFFR cable layer (280°C). Table 4 also indicates that the measured Vf are higher for the preheated PVC cable layers (0 to 5.5 mm/s) than for the preheated HFFR cable layer (0 to 1.5 mm/s) while T_s values are lower for the preheated PVC cable layers (170 to 250°C) than for the preheated HFFR cable layer (280 to 370°C). The whole above outcomes are consistent with the classification of the PVC cable (low-qualified) and that of the HFFR cable (well-qualified). Similar trends were obtained between PVC and HFFR cables in work [14] that measured vertical flame spread velocities in the 3 to 24 mm/s range for a preheated (22 to 190°C) PVC cable and in the 0 to 4 mm/s range for a preheated (22 to 293°C) HFFR cable.

Finally, when examining both Figure 15A and C, it appears that for a given T_s higher than 210°C, Vf is slightly higher for the wider PVC cable layer. The fire of the latter layer is indeed assumed leading to a larger flame front that would increase the flame heat flux to the unburnt cables and thus would accelerate the flame spread. This result cannot be unfortunately confirmed by the $\dot{q}''_f$ increase observed between the last test of series2 and first test of series4 (Figure 16) since two parameter changed between the latter (the cable layer width and the cable type). Furthermore, it can be noticed that the maximum Vf for the 11 and 22 cm wide cable layers are both close to 5.5 mm/s. This value was indeed obtained for a higher T_s (244°C) for the 11 cm wide cable layer (Figure 15A) than those implemented (232 and 234°C) for the wider cable layer (Figure 15C). Finally, it is worth noting that the Vf measurement ranges [0 to 5.5 mm/s] on the PVC cable layers are consistent with those [0 to 5 mm/s] obtained on the horizontal cable trays of the real-scale fire tests that used the same PVC cable [28]. These first outcomes are promising regarding the representativeness of the flame spread experiments using the CISCCO test device.

5.2. *Effect of the Cable Preheating on the Heat Release Rate (Series4)*

This section discusses the effect of the cable preheating on the HRR that was measured only for the last test series. Figure 17 shows the HRR for all tests of series4 that were performed for T_s measured in the 200 to 235°C range. This figure exhibits that the peak of the HRR, $pHRR$, increases with T_s. The following linear correlation (coefficient of determination, $R^2 = 0.88$) is shown between these two parameters (Figure 18):$pHRR = 0.738 \cdot T_s - 121.5$ ($pHRR$ is given in kW). The $pHRR$ values for all tests of series4 are provided in Table 5. The latter table also reports the times to reach $pHRR$ from the onset of the fire, t_{pHRR} (s), and the cable fire growth rate, CFGR (kW/s), especially specified for the CISCCO flame spread experiments, as follows:

Table 4
Additional Outcomes of the Temperature Dependence of the Flame Spread Velocity for the Three Studied Cable Layers

Parameter	11 cm wide PVC cable layer (series1&3)	22 cm wide PVC cable layer (series4)	11 cm wide HFFR cable layer (series2)
$T_{s,min}$(C)	170	<200	280
Studied T_s range	[170 to 250°C]	[200 to 235°C]	[280 to 370°C]
Studied Vf range	[0 to 5.5 mm/s]	[0.5 to 5.5 mm/s]	[0 to 1.5 mm/s]

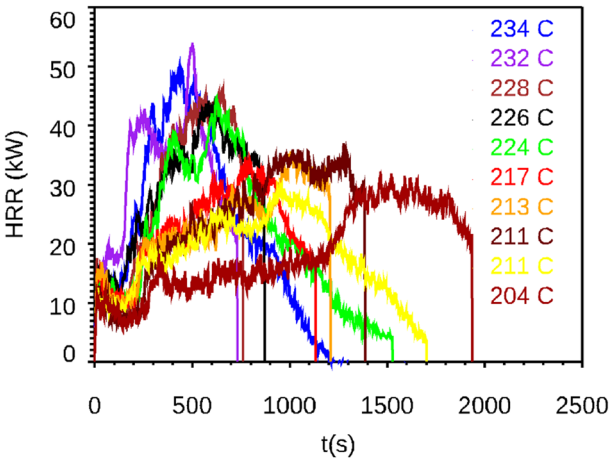

Figure 17. Heat release rate (HRR) measured for all tests of series4 (t = 0 s corresponds to the cable ignition time for all tests).

$$CFGR = \frac{pHRR}{t_{pHRR}} \tag{11}$$

Figure 19 gives CFGR as a function of T_s, revealing its temperature dependence according to the following power law:

$$CFGR = \frac{0.08}{(260 - T_s)^2} \tag{12}$$

This law is similar to the temperature dependence law for Vf of series4 (Equation (9) and Table 3). Finally, the below linear correlation ($R^2 = 0.93$) is found between these two fire dynamic parameters (Figure 20):

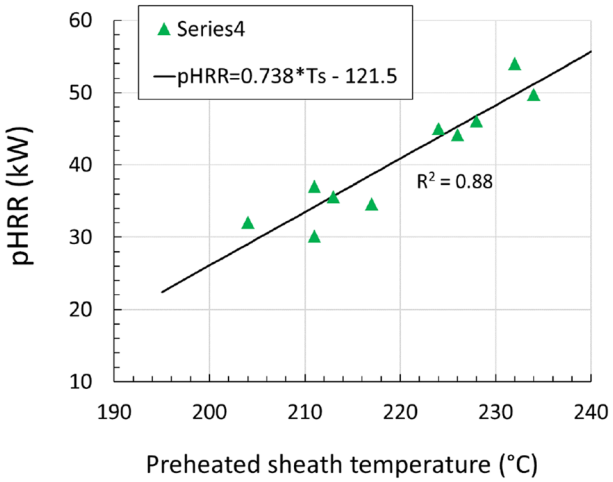

Figure 18. Peak of the HRR (pHRR) as a function of the preheated sheath temperature (series4).

Table 5
Peaks of the Heat Release Rate (HRR) and of the Cable Fire Growth Rate (CFGR) for Series4

Test ID of series4	Preheated sheath temperature, T_s (°C)	Peak of HRR, *pHRR*, (kW)	Time to reach the peak of HRR, t_{pHRR} (*s*)	Cable fire growth rate, CFGR (kW/s)
Test 1	204	32.1	1466	0.022
Test 2	211	30.2	954	0.032
Test 3	211	37	1277	0.029
Test 4	213	35.6	1006	0.035
Test 5	217	34.6	773	0.045
Test 6	224	45	623	0.072
Test 7	226	44.2	585	0.076
Test 8	228	46.1	658	0.070
Test 9	232	54.0	502	0.108
Test 10	234	49.8	432	0.115

$$Vf = 49.5 \cdot CFGR \tag{13}$$

The appropriateness of the latter correlation can be substantiated such as developed below. The HRR of a cable layer fire can be assessed as follows [5]:

$$HRR = A_b \cdot HRRPUA \tag{14}$$

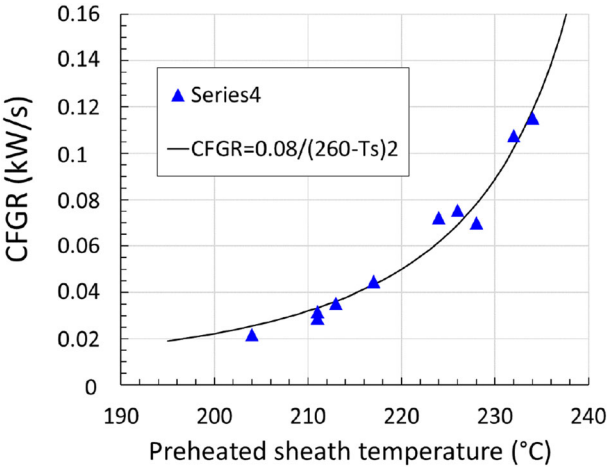

Figure 19. Cable fire growth rate (CFGR) as a function of the preheated sheath temperature (series4).

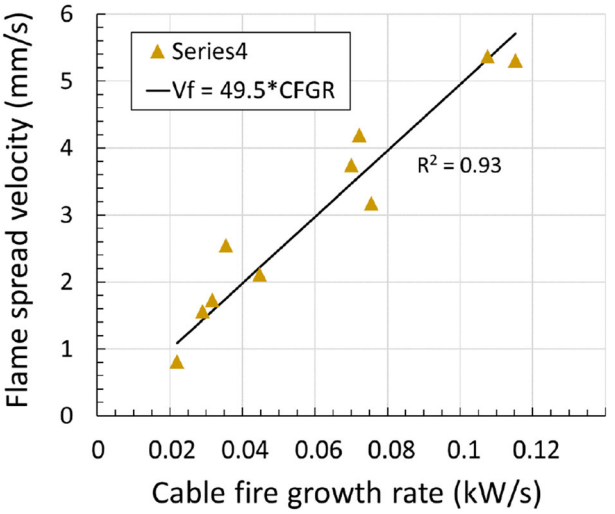

Figure 20. Flame spread velocity (*Vf*) as a function of the cable fire growth rate (CFGR).

where A_b is the burning area of the cable layer (m^2) and *HRRPUA*, the average heat release rate per unit area of the cable layer fire (kW/m^2). Furthermore, assuming a steady flame spread along the cable layer, Equation (14) can be written as:

$$HRR = w \cdot Vf \cdot t \cdot HRRPUA \tag{15}$$

where w is the cable layer width and t, the time from the ignition. Thus, Vf can be expressed:

$$Vf = \frac{1}{w \cdot HRRPUA} \cdot \frac{HRR}{t} \tag{16}$$

The steady flame spread assumption also implies that the HRR grows linearly with t (Equation (15)). Accordingly, the latter equation can be written:

$$Vf = \frac{1}{w \cdot HRRPUA} \cdot \frac{pHRR}{t_{pHRR}} = \frac{1}{w \cdot HRRPUA} \cdot CFGR \tag{17}$$

To complement this analysis, given w = 22 cm for the PVC cable layer width used for series4 and the average HRRPUA for the studied PVC cable measured in the cone calorimeter at about 105 kW/m^2 [28], $1/w \cdot HRRPUA$ gives 43.5 mm/kW. This value is consistent with the coefficient 49.5 of the above correlation (Equation (13)).

6. Conclusions

The new CISCCO test device was developed to conduct flame spread experiments on a preheated horizontal cable layer to support the development and validation of cable fire models. Four test series were conducted to first investigate the temperature dependence of the flame spread velocity. Test series1, 2 and 3 used a 11 cm wide cable layer while test series4 involved a 22 cm wide cable layer. Test series1, 3 and 4 used the same polyvinyl chloride (PVC)-based cable, named PVC cable, while test series2 used a halogen free flame retardant (HFFR) and poly (ethylene–vinyl acetate)/polyethylene-based cable, labelled HFFR cable. The PVC and HFFR cables are considered as a low-qualified (LQ) cable and a well-qualified (WQ) cable, respectively, since the former meets the requirement of only one not challenging fire standard while the latter satisfies several and more demanding fire standards. Temperature measurements performed in the solid phase (cable outer sheath) and in the gas phase (above the cable layer) allowed to assess the preheated cable layer temperature and the flame spread velocity. A first attempt of flame heat flux measurements was also conducted in this work.

All series highlighted a temperature dependence of the flame spread velocity, Vf, according to experimental power laws. The tests also revealed that the minimal sheath temperature leading to the flame spread was notably lower for the 11 cm wide PVC cable layer (170°C) than for the 11 cm wide HFFR cable layer (280°C). In addition, Vf were measured higher for the preheated PVC cable layers (0 to 5.5 mm/s) than for the preheated HFFR cable layer (0 to 1.5 mm/s) while the related preheated sheath temperatures, T_s, are lower for the preheated PVC cable layers (170 to 250°C) than for the preheated HFFR cable layer (280 to 370°C). The whole above outcomes are consistent with the classification of the PVC cable (low-qualified) and that of the HFFR cable (well-qualified). Furthermore,

for a given T_s higher than 210°C, it appears that the wider the PVC cable layer, the higher the flame spread velocity, under the conditions of the tests. However, regardless of the width of the cable layer, Vf of the PVC cable layers remains in the same order of magnitude [0 to 5.5 mm/s] than that measured during previous real-scale cable tray fire experiments using the same PVC cable [0 to 5 mm/s]. Furthermore, the last test series that used the 22 cm wide PVC cable layer and implemented heat release rate (HRR) measurements studied the impact of the cable preheating on HRR. First, it was shown that the HRR peak increases linearly with T_s. This series also showed that the cable fire growth rate (CFGR), such as specified in the CISCCO experiments, is dependent on T_s according to a power law similar to that for Vf. A linear correlation between CFGR and Vf was finally proposed.

Acknowledgements

The authors thank V. Lemaux and F. Vigroux for the preparation and performance of the tests. The authors are also grateful to Electricité de France (EdF) that sponsored this work through a bilateral partnership with IRSN.

References

1. Aprin L, Ferry L, Heymes F, Sonnier R, Zavaleta P (2022) Chapter 9—Correlation between laboratory- and real-scale fire analyses. Analysis of flame retardancy in polymer science Elsevier, , pp 333–379
2. Organisation for Economic Co-operation and Development (OECD) Nuclear Energy Agency (NEA), Committee on the Safety of Nuclear Installations (CSNI) (2021) OECD/NEA FIRE Database Version 2019:01, Paris, France (limited to FIRE Database Project member countries only)
3. Keski-Rahkonen O, Mangs J (2002) Electrical ignition sources in nuclear power plants: statistical, modelling and experimental studies. Nucl Eng Des 213:209–221
4. McGrattan K, Lock A, Marsh N, Nyden M, Bareham S, Price M, Morgan AB, Galaska M, Schenck K, Stroup D (2012) Cable heat release, ignition, and spread in tray installations during fire (CHRISTIFIRE), vol 1: Horizontal trays, NUREG/CR-7010, U.S.NRC
5. Zavaleta P, Hanouzet R, Beji T (2019) Improved assessment of fire spread over horizontal cable trays supported by video fire analysis. Fire Technol 55:233–255. 10.1007/s10694-018-0788-x
6. Zavaleta P, Suard S, Audouin L (2019) Cable tray fire tests with halogenated electric cables in a confined and mechanically ventilated facility. Fire Mater 43:543–560. 10.1002/fam.2717

7. Fernandez-Pello AC, Hirano T (1983) Controlling mechanisms of flame spread. Combust Sci Technol 32(1–4):1–31. 10.1080/00102208308923650
8. Quintiere J (2002) Surface flame spread. In: Chapter 12—SFPE handbook of fire protection engineering, Sect. 2, 3rd edn., pp. 246–257
9. Gollner MJ, Miller CH, Tang W, Singh AV (2017) The effect of flow and geometry on concurrent flame spread. Fire Saf J 91:68–78. 10.1016/j.firesaf.2017.05.007
10. deRis JN (1969) Twelfth international symposium on combustion. The Combustion Institute, Pittsburgh, p. 241
11. Kobayashi Y, Konno Y, Huang X, Nakaya S, Tsue M, Hashimoto N, Fujita O, Fernandez-Pello C (2018) Effect of insulation melting and dripping on opposed flame spread over laboratory simulated electrical wires. Fire Saf J 95:1–10. 10.1016/j.firesaf.2017.10.006
12. Hu L, Zhang Y, Yoshioka K, Izumo H, Fujita O (2015) Flame spread over electric wire with high thermal conductivity metal core at different inclinations. Proc Combust Inst 35:2607–2614. 10.1016/j.proci.2014.05.059
13. Wang Z, Wang J (2020) A comprehensive study on the flame propagation of the horizontal laboratory wires and flame-retardant cables at different thermal circumstances. Process Saf Environ Prot 139:325–333. 10.1016/j.psep.2020.04.030
14. Mangs J, Hostikka S (2013) Vertical flame spread on charring materials at different ambient temperatures. Fire Mater 37:230–245. 10.1002/fam.2127
15. Atreya A, Carpenter C, Harkleroad M (1985) Effect of sample orientation on piloted ignition and flame spread, fire safety science. In: Grant CE, Pagni PJ (eds) Proceedings of the first international symposium, international association for fire safety science Hemisphere Publishing Corp, NY, p 97
16. Meinier R (2021) Étude expérimentale et analytique de l'inflammation et de la propagation du feu sur un chemin de câbles électriques. IMT Mines Alès,
17. Vincent C, Corn S, Longuet C, Aprin L, Rambaud G, Ferry L (2019) Experimental and numerical thermo-mechanical analysis of the influence of thermoplastic slabs installation on the assessment of their fire hazard. Fire Saf J 108:102850. 10.1016/j.firesaf.2019.102850
18. Meinier R, Sonnier R, Zavaleta P, Suard S, Ferry L (2018) Fire behavior of halogen-free flame retardant electrical cables with the cone calorimeter. J Hazard Mater 342:306–316. 10.1016/j.jhazmat.2017.08.027
19. Meinier R, Fellah M, Sonnier R, Zavaleta P, Suard S, Ferry L (2022) Ignition and charring of PVC-based electric cables. Fire Technol 58:689–707. 10.1007/s10694-021-01168-0
20. IEC 60332-1-2. Tests on electric and optical fibre cables under fire conditions—Part 1–2: test for vertical flame propagation for a single insulated wire or cable—procedure for 1 kW pre-mixed flame. International Electrotechnical Commission (IEC)
21. BS EN 50575:2014 + A1:2016. Power, control and communication cables: cables for general applications in construction works subject to reaction to fire requirements
22. IEC 60332-3-23. Tests on electric cables under fire conditions—Part 3–23: test for vertical flame spread of vertically-mounted bunched wires or cables—Category B. International Electrotechnical Commission (IEC)
23. NF C32-070, Janvier 2001, Conducteurs et câbles isolés pour installations, Essais de classification des conducteurs et câbles du point de vue de leur comportement au feu, AFNOR
24. IEC/EN 61034-2. Measurement of smoke density of cables burning under defined conditions—Part 2: test procedure and requirements. International Electrotechnical Commission (IEC)

25. IEC/EN 60754-2. Test on gases evolved during combustion of materials from cables—Part 2: determination of acidity (by pH measurement) and conductivity. International Electrotechnical Commission (IEC)
26. Zavaleta P, Audouin L (2018) Cable tray fire tests in a confined and mechanically ventilated facility. Fire Mater 42:28–43. 10.1002/fam.2454
27. Boulet P, Parent G, Acem Z, Collin A, Försth M, Bal N, Rein G, Torero J (2014) Radiation emission from a heating coil or a halogen lamp on a semitransparent sample. Int J Therm Sci 77:223–232. 10.1016/j.ijthermalsci.2013.11.006
28. Pretrel H, Zavaleta P, Suard S (2022) Experimental investigation of the effects of a sidewall and cable arrangement on a horizontal cable tray fire in an open atmosphere. Fire Mater . 10.1002/fam.3114
29. Zavaleta P, Bascou S, Suard S (2017) Effects of cable tray configuration on fire spread. In: Proceeding of the fifteenth international fire and materials conference. San Francisco, pp. 17–30
30. Quintiere JG (1993) A simulation model for fire growth on materials subject to a room-corner test. Fire Saf J 20:313–339. 10.1016/0379-7112(93)90053-S
31. Girardin B, Fontaine G, Duquesne S, Forsth M, Bourbigot S (2015) Characterization of thermo-physical properties of eva/ath: application to gasification experiments and pyrolysis modeling. Materials 161:7837–7863
32. Shi J, Boyer G, Mourzenko V, Thovert JF (2020) Evolutive models for the geometry and heat conductivity of an intumescent eva-ath composite during its thermal degradation. Materials 13:5258
33. Shi J, Boyer G, Mourzenko V, Thovert JF (2023) A comprehensive numerical model for the pyrolysis of intumescent polymers: application to EVA-ATH compounds. Chem Eng Sci 268:118385